



A Kinematic Wave Model for Rivers with Flood Plains and Other Irregular Geometries

P. M. JACOVKIS*

Instituto de Cálculo and Departamento de Computación
Facultad de Ciencias Exactas y Naturales, Universidad de Buenos Aires
Buenos Aires, Argentina

E. G. TABAK†

Courant Institute of Mathematical Sciences, NYU
251 Mercer Street, New York, NY 10012, U.S.A.

(Received March 1996; accepted May 1996)

Abstract—A general kinematic wave model for flood propagation is presented in the form of a scalar conservation law. The corresponding flux function is convex or nearly convex for regular cross-sections of the river. In the presence of pronounced irregularities, however, convexity may fail. Qualitative consequences of the shape of the flux function for typical irregularities are discussed, particularly for rivers with flood plains and rivers trapped in canyons.

Keywords—Flood waves, Kinematic waves, Conservation laws, Flood plains.

1. INTRODUCTION

The one-dimensional gradually varied unsteady water flow in open channels or rivers with arbitrary cross-sections and fixed bed is governed by the Saint-Venant hydrodynamic equations

$$\frac{\partial S}{\partial t} + \frac{\partial Q}{\partial x} = 0, \quad (1)$$

$$\frac{\partial}{\partial t} \left(\frac{Q}{S} \right) + \frac{1}{2} \frac{\partial}{\partial x} \left(\frac{Q}{S} \right)^2 + g \frac{\partial Z}{\partial x} + \frac{Q |Q|}{D^2} = 0, \quad (2)$$

where x is the spatial longitudinal coordinate, t is the time, $Q = Q(x, t)$ is the discharge, $S = S(Z(x, t), x)$ is the wetted cross-section, $Z = Z(x, t)$ is the surface level measured from a fixed plane of reference, g is the acceleration of gravity, and $D = D(Z(x, t), x)$ is the conveyance, conveniently related to the frictional resistance to the flow (see Figures 1 and 2).

Equations (1) and (2) represent conservation of mass and momentum, respectively. With suitable initial and boundary conditions, they form a mixed initial-boundary value quasilinear hyperbolic system of partial differential equations. A careful derivation of equations (1) and (2) can be found in [1], and Liggett and Cunge [2] describe several methods used for their numerical solution.

From a practical point of view, the main problem that arises while modeling a reach of a river is the calibration of the conveyances $D(Z(x, t), x)$, that usually cannot be measured. For

*The author gratefully acknowledges the support of the Universidad de Buenos Aires through Grant EX107.

†Work partially supported by the National Science Foundation through Grant DMS 9501073.

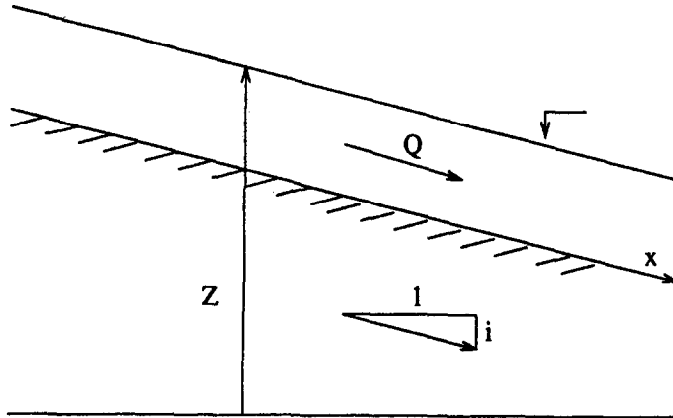


Figure 1. Schematic longitudinal section of a river. The variable x measures the length along the river, Z is the height of the water surface from a fixed horizontal reference plane, i is the surface slope, and Q the water flux per unit time.

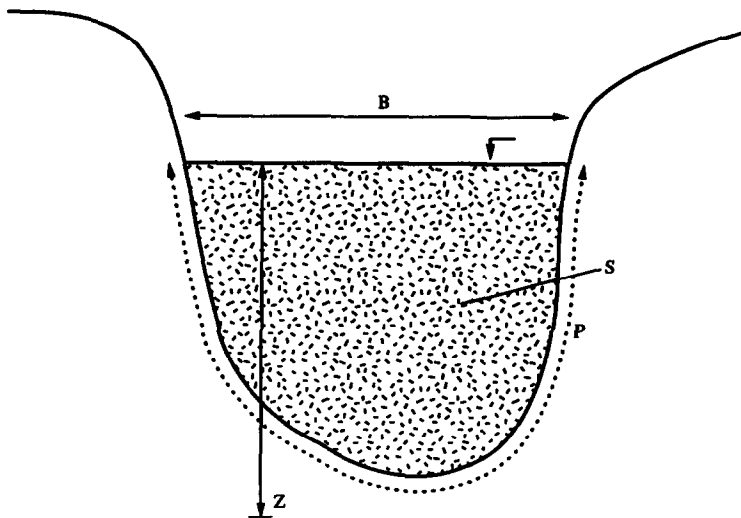


Figure 2. Schematic cross-section of a river. The variable S represents the wetted area, P the wetted perimeter, and B the surface width.

ivers with very irregular cross-sections, it is difficult to represent conveyances by means of simple functions, so in general it is necessary to resort to tables. Then a large number of parameters must be calibrated, a time-consuming and complex task. Besides, many field data are necessary which may not be available. For these reasons, rivers are sometimes successfully modeled with the simplifying assumption that a one-to-one discharge/surface level function exists at each point of the reach. With this closure hypothesis, we use only equation (1) and, as S is a one-to-one function of Z , we have $Q(x, t) = Q(S(x, t), x)$, so (1) becomes

$$\frac{\partial S}{\partial t} + \frac{\partial Q(S, x)}{\partial S} \frac{\partial S}{\partial x} + \frac{\partial Q(S, x)}{\partial x} = 0. \quad (3)$$

This kinematic wave equation, which has been studied in [3], can be derived from the complete system (1),(2) under the closure hypothesis that S and Q vary on very long spatial and temporal

scales, in a nondimensionalization based on the gravitational and frictional forces. Under this hypothesis, the first two terms in equation (2) drop out, the third term $g\frac{\partial Z}{\partial x}$ is replaced by gi , where i is the slope at the bottom, and the conveyance D becomes a function of S . Thus, (2) provides a relation between Q and S which, replaced in (1), yields equation (3). This quasilinear hyperbolic differential equation has many advantages over the complete system (1),(2), since it is much simpler conceptually, and the number of parameters to calibrate is relatively small.

Of course, the results obtained have much less precision than those that could be produced with a complete modeling of equations (1),(2), but one often has not the field data to feed the complete model anyway, so equation (3), with initial condition

$$S(x, t_0) = S_0(x), \quad (4)$$

and boundary condition at the upstream extreme point x_0

$$S(x_0, t) = f(t) \quad (5)$$

is sufficient for many purposes. In fact, many kinematic models have been developed and many have been commercially implemented in the last thirty years. Often these models are combined with others (for instance, with rainfall-run off or with overbank flooding models) to obtain a more efficient tool. An impressive mass of bibliography exists, that may be found in engineering journals, reports, and proceedings of conferences; we mention, for instance, [4–6]. Among the models used commercially, we may mention the very popular HEC models developed by the U. S. Army Corps of Engineers [7], which are continually completed and updated (see, for instance, [8]).

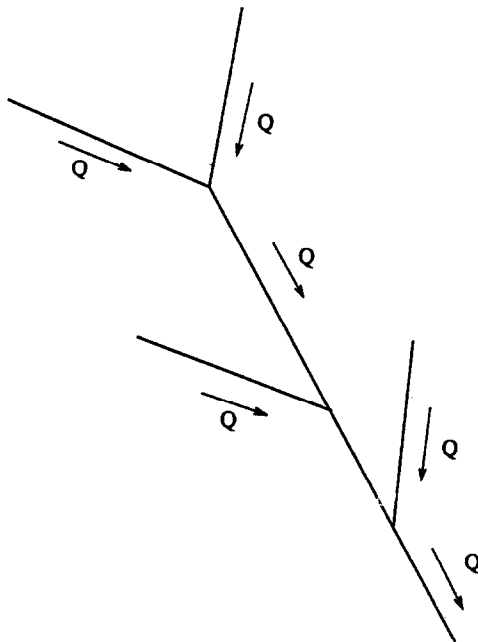


Figure 3. An arborescent river. Conservation of mass must be enforced at each junction.

Notice that, with this kinematic wave, or using engineering terminology, this hydrologic or flood routing model, we may model not only reaches of rivers or channels, but also basins with arborescent structures (see Figure 3). We only need to solve numerically each tributary reach separately and, at the junction points, use conservation of mass

$$Q_i + Q_j = Q_k,$$

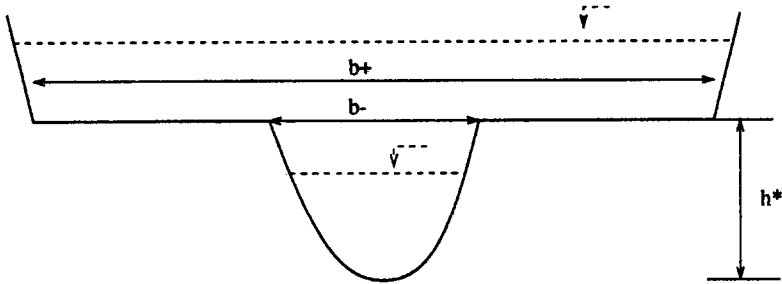


Figure 4. Schematic cross-section of a river with flood plains.

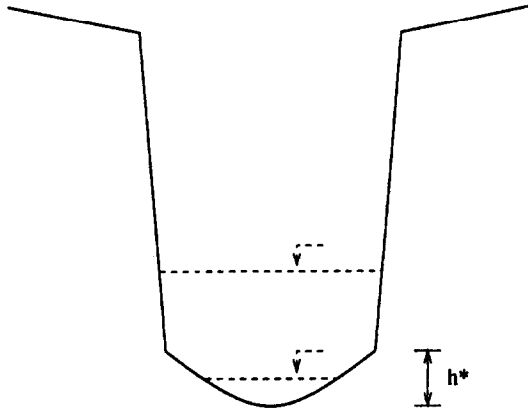


Figure 5. Schematic cross-section of a river trapped in a canyon.

where Q_i and Q_j are the computed values of discharges at the end of reaches i and j , and Q_k is the value of the discharge at the beginning of reach k , that acts as upstream boundary condition for that reach. External boundary conditions are needed at each open upstream extreme point, and depending nonlinearly on the solution, at some of the downstream extreme points. To deal with the arborescent case with the complete system (1),(2), a more complex procedure is required, as may be seen in [9].

If we assume that the discharge/surface level function is the same for all the points of the reach, namely, that $Q = Q(S)$ (that would be the case for an approximately prismatic channel), we may write (3) as

$$\frac{\partial S}{\partial t} + \frac{\partial Q(S)}{\partial x} = 0, \quad (6)$$

which is a scalar conservation law with a generally nonlinear flux Q [10].

In this paper, we discuss the qualitative features of the flux function $Q(S)$ for rivers and channels with various typical cross-sections. In particular, we show that the flux functions for rivers with flood beds (Figure 4), and rivers trapped in canyons (Figure 5) have some very distinctive features, which determine a very rich and peculiar phenomenology. We remark that this is not a theoretical exercise: there are natural rivers with geometries very similar to those drawn in Figures 4 and 5; we may mention, for instance, the Paraná de las Palmas River in Argentina and the Ottauquechee River in Vermont, respectively. Although a realistic flood simulation for any of these rivers would require the use of the full system (1),(2), we shall present evidence here that even a simple kinematic model yields surprisingly rich predictions.

2. A KINEMATIC WAVE MODEL FOR PRISMATIC CHANNELS

We mean by a prismatic channel, one with constant cross-section. If we assume that the bed material is the same for all levels of water and all longitudinal coordinates x , we may compute a one-to-one function $Q(S)$ by using the Chézy hypothesis that the friction resistance τ is

proportional to the square of the mean velocity $V = Q/S$

$$\tau = f\rho PV^2,$$

where f is a friction coefficient, ρ the density of water, and P the wetted perimeter (see Figures 1 and 2).

Following Lighthill and Whitham, we balance the resistance τ with the x -component F_x of gravity which, for small reach slope i , can be written as

$$F_x = ig\rho S.$$

Then, we have

$$V = \sqrt{\frac{igS}{fP}} = M\sqrt{\frac{S}{P}},$$

where $M = \sqrt{ig/f}$. Therefore,

$$Q = VS = M\frac{S^{3/2}}{P^{1/2}}. \quad (7)$$

Note that in this model, we have only one parameter to calibrate, namely f , or equivalently M .

Let us analyze now the expressions for $\frac{dQ}{dS}$ and $\frac{d^2Q}{dS^2}$. We have

$$\frac{dQ}{dS} = M \left(\frac{3}{2} \left(\frac{S}{P} \right)^{1/2} - \frac{1}{2} \left(\frac{S}{P} \right)^{3/2} \frac{dP}{dS} \right), \quad (8)$$

$$\frac{d^2Q}{dS^2} = \frac{3M}{4(SP)^{1/2}} \left(\left(1 - \frac{S}{P} \frac{dP}{dS} \right)^2 - \frac{2}{3} \frac{S^2}{P} \frac{d^2P}{dS^2} \right). \quad (9)$$

It follows from (9) that, if $\frac{d^2P}{dS^2} < 0$, then Q is a strictly nonlinear convex function of S . Conditions for existence and unicity of solutions in this case are discussed in [1].

It is worth noticing that, for “normal” cross-sections, $\frac{d^2P}{dS^2} < 0$ holds, and therefore, $Q(S)$ is a convex function. To see this, let us consider a symmetric cross-section, and represent its right boundary in the plane (h, b) , as shown in Figure 6, where h is the height and $b(h)$ is the transversal coordinate with origin in the axis of symmetry of the cross-section, so the free-surface width at height h is $2b(h)$. For “normal” cross-sections, the function $b(h)$ is concave. In that case, if $b(h)$ is a concave nondecreasing function, $Q(S)$ is convex. To prove this, we need only show that $\frac{d^2P}{dS^2} < 0$. By hypothesis, $\frac{d^2b}{dh^2} \leq 0$ and $\frac{db}{dh} \geq 0$. Then, assuming without loss of generality that $b(0) = 0$, we have

$$\begin{aligned} S(h) &= 2 \int_0^h b(\eta) d\eta, \\ P(h) &= 2 \int_0^h \sqrt{\left(\frac{db}{d\eta} \right)^2 + 1} d\eta, \\ \frac{dP}{dS} &= \frac{db}{dS} = \frac{\sqrt{\left(\frac{db}{dh} \right)^2 + 1}}{b}, \\ \frac{d^2P}{dS^2} &= \frac{\frac{db}{dh}}{2b^3 \sqrt{\left(\frac{db}{dh} \right)^2 + 1}} \left(b \frac{d^2b}{dh^2} - \left(\frac{db}{dh} \right)^2 - 1 \right) < 0. \end{aligned}$$

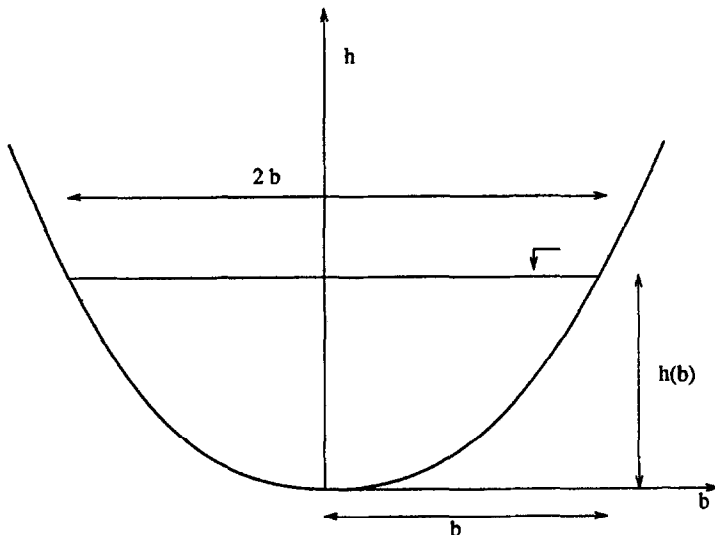


Figure 6. A symmetric cross-section.

Note that the last inequality holds for a simple shape given by $b(h) = kh^r$, not only for the concave cases with $r \leq 1$, but for all positive r 's, which includes a large family of nonconcave functions.

Let us consider now the case of a trapezoidal cross-section, like the one represented in Figure 7. If α is the angle between the lateral wall of the cross-section and the horizontal transversal axis, with $0 < \alpha < \frac{\pi}{2}$, and B_0 is the bed width, we have

$$S(h) = (B_0 + h \cot(\alpha)) h, \quad (10)$$

$$P(h) = B_0 + 2h \csc(\alpha). \quad (11)$$

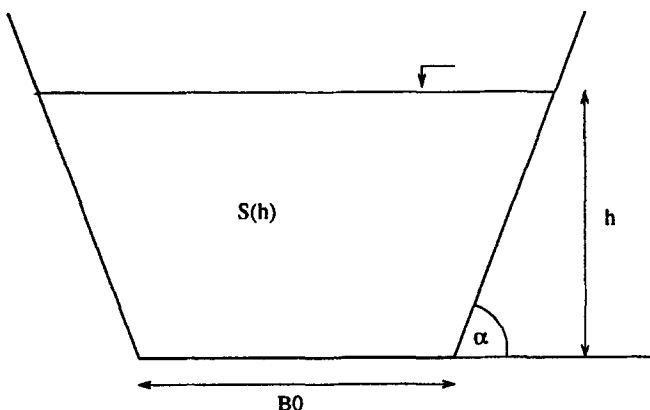


Figure 7. A trapezoidal cross-section.

From (10) and (11), we compute

$$\frac{dP}{dS}(h) = \frac{2 \csc(\alpha)}{B_0 + 2h \cot(\alpha)},$$

$$\frac{d^2P}{dS^2}(h) = -\frac{4 \csc(\alpha) \cot(\alpha)}{(B_0 + 2h \cot(\alpha))^3} \leq 0.$$

Therefore, if the cross-section is a trapezoid and the surface width is an increasing function of the height, $Q = Q(S)$ given by (7) is a convex function.

If the width is a decreasing function of the height, however, a straightforward calculation shows that the flux function is not convex. This curious fact has interesting consequences for underground rivers, where the width of the free surface is not monotonically increasing. However, we will not pursue this line of study here.

3. A PIECEWISE TRAPEZOIDAL CROSS-SECTION

Let us analyze a piecewise trapezoidal cross-section, as indicated in Figure 8. The reason for considering such cross-sections is that they are easy to compute, and yet in some sense general, since any cross-section can be approximated by a piecewise trapezoidal one. For simplicity of the exposition, we will consider only symmetric cross-sections.

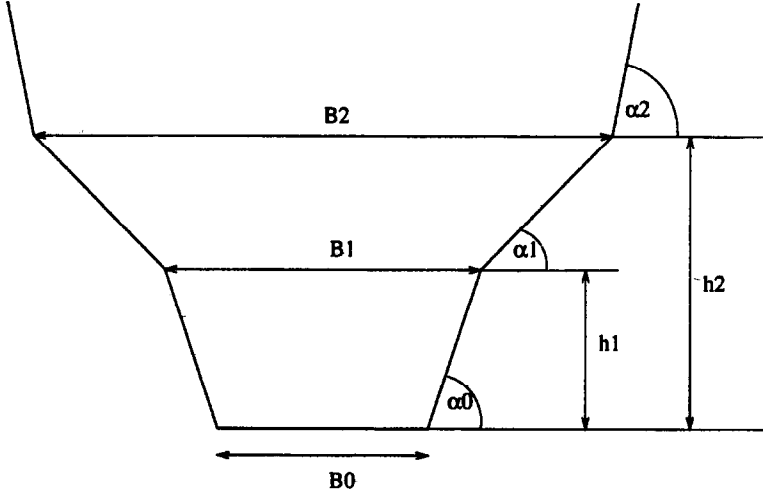


Figure 8. A piecewise trapezoidal cross-section.

If h_i is the height at which the lateral slope changes (h_0 being the bed height), and α_i, B_i, S_i, P_i the corresponding angles, widths, cross-section wetted areas, and wetted perimeters, respectively, with $P_0 = B_0, S_0 = 0, 0 < \alpha_i \leq \frac{\pi}{2}$, we have, for $h_i \leq h < h_{i+1}, i \geq 0$,

$$\begin{aligned} S(h) &= S_i + (B_i + (h - h_i) \cot(\alpha_i))(h - h_i), \\ P(h) &= P_i + 2(h - h_i) \csc(\alpha_i), \\ \frac{dP}{dS} &= \frac{2 \csc(\alpha_i)}{B_i + 2(h - h_i) \cot(\alpha_i)}, \\ \frac{d^2P}{dS^2} &= -\frac{4 \csc(\alpha_i) \cot(\alpha_i)}{(P_i + 2(h - h_i) \cot(\alpha_i))^3} \leq 0. \end{aligned}$$

Therefore, the flux $Q(S)$ is piecewise convex. However, it will generally have slope discontinuities at the points S_i , which will in some cases make $Q(S)$ globally nonconvex. To see this, note from (8) that

$$\frac{dQ_i^-}{dS} > \frac{dQ_i^+}{dS} \iff \frac{dP_i^-}{dS} < \frac{dP_i^+}{dS},$$

where the superindices + and - refer to the slopes immediately above and below S_i . On the other hand,

$$\frac{dP_i^-}{dS} = \frac{2 \csc(\alpha_{i-1})}{B_i},$$

and

$$\frac{dP_i^+}{dS} = \frac{2 \csc(\alpha_i)}{B_i},$$

so that

$$\frac{dP_i^-}{dS} < \frac{dP_i^+}{dS} \iff \csc(\alpha_{i-1}) < \csc(\alpha_i),$$

that is, if and only if $\alpha_{i-1} > \alpha_i$.

We conclude that the flux $Q(S)$ for a symmetric piecewise trapezoidal cross-section will be convex if and only if the cross-section itself is convex. If this is not the case, i.e., if at any point h_i the lateral slope decreases with the altitude, $Q(S)$ will be nonconvex, with a local behavior of the kind represented in Figure 9a. On the other hand, at those points where the section is convex but the lateral slopes change abruptly, $Q(S)$ will be convex but will possess a sharp corner, as displayed in Figure 9b. We will see in later sections how these features of the flux affect the behavior of the solutions to (6).

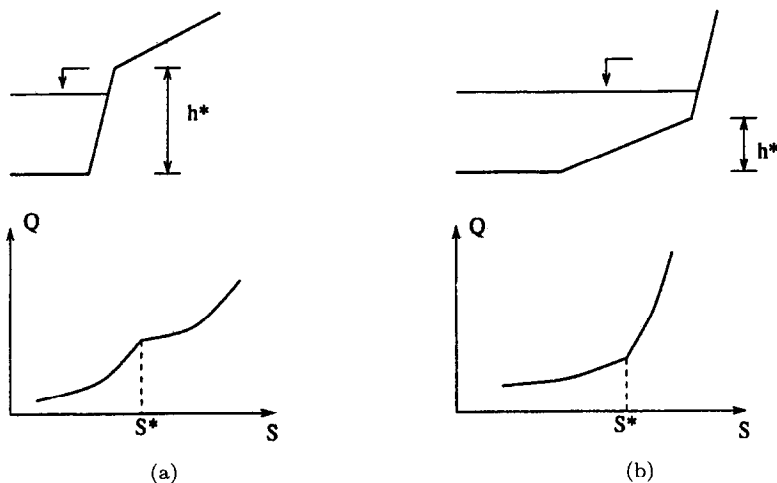


Figure 9. Nonconvex and convex corners, with corresponding shape of the flux functions.

4. RIVERS WITH FLOOD PLAINS AND RIVERS TRAPPED IN CANYONS

With the tools developed above, we could now, in principle, analyze cross-sections of any kind, by approximating them by piecewise trapezoidal profiles. We must, nevertheless, be careful to check in each situation whether the physical assumptions of the model really apply. If they do not, we may want to modify the model to take the new features into account. In this section, we concentrate on finding the qualitative features of the flux function $Q(S)$ for two important kinds of rivers: those with flood plains and those trapped in canyons. We will see that the latter can be well described by the piecewise trapezoidal model, while the former requires some further refinements.

Large plain rivers, such as the Paraná de las Palmas in Argentina, often have a regular basin, where the water stays most of the time, and a much wider flood plain, where water only flows on the occasion of exceptional rains or thaw upstream. The cross-section of such rivers has a profile like the one sketched in Figure 4. There is a critical height h^* , below which the river flows within its regular basin, and above which flooding occurs. We would like to study the qualitative features of the transition between the two regimes, in the simple model of the kinematic wave approximation. If we were to use the Chézy model of Section 2, we would find that the flux $Q(S)$ is discontinuous across the critical area S^* . This can be seen directly from equation (7): as the height of water crosses h^* , the area S changes continuously, but the wetted perimeter P jumps, by the addition of the whole flat bottom of the flood bed. Then the friction increases, while the driving gravity force remains basically constant, therefore, causing a finite drop in the discharge Q . The same result is obtained as a limiting case of the piecewise trapezoidal section, if we consider a bed of the flood basin with a small slope, and let this slope go to zero. Schematic plots of $Q(S)$ from these two procedures are depicted in Figure 10.

Is this discontinuity of $Q(S)$ realistic? Can the friction at the flood plain suddenly slow down the flow of water through the main basin? The answer to this question would be positive if water

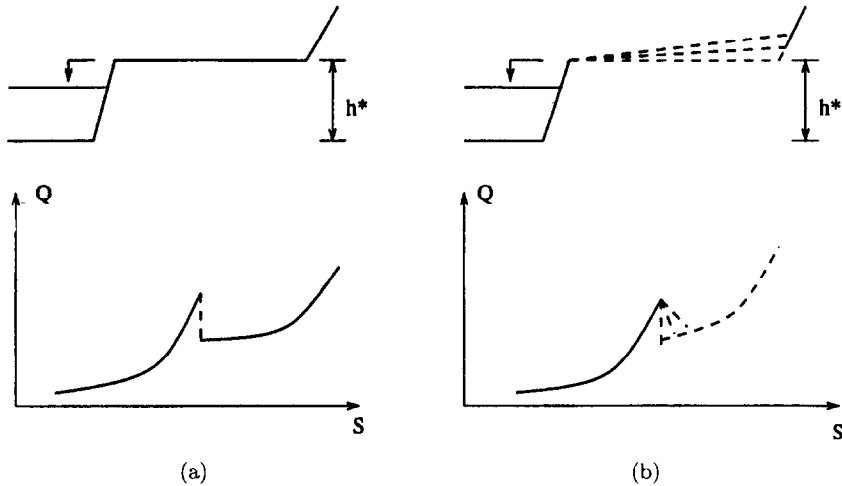


Figure 10. A Chézy model with uniform mean velocity for a river with flood plains, with and without bed slopes.

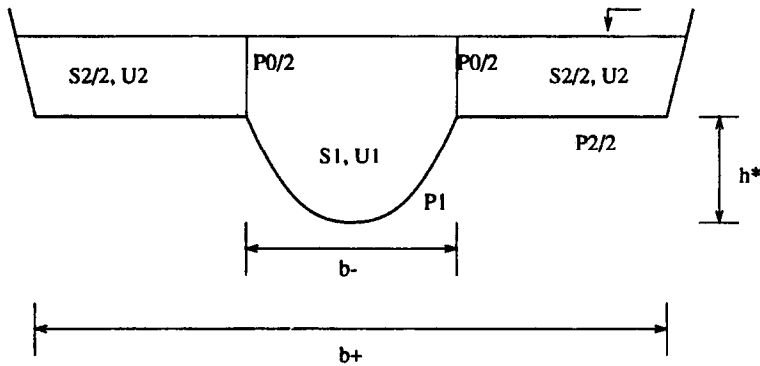


Figure 11. Improved model for a river with flood plains, with two mean velocities.

were viscous to the point of looking semisolid: then the central flow would immediately perceive the added friction, and slow down accordingly. But this is not the case. The friction at the bottom of the flood bed can make the velocity of water at the flood bed itself very slow, but it cannot slow down the flow through the main basin. Therefore, it is the hypothesis of a uniform mean flow which fails. A better model should include two mean velocities, one inside the main basin and another at the lateral beds.

A sketch of the improved model is plotted in Figure 11. There are two mean velocities U_1 and U_2 , two areas S_1 and S_2 , two wetted perimeters P_1 and P_2 , plus the interface between the two areas P_0 . For each area, we can write the balance between frictional and gravitational forces, with the velocities coupled through the frictional forces at the interface P_0 . For each height h , we can write $S(h) = S_1(h) + S_2(h)$ and $Q(h) = U_1(h)S_1(h) + U_2(h)S_2(h)$, and thus, compute the flux $Q(S)$. The details are easy to work out. For the purposes of this paper, however, it is enough to notice the following two qualitative facts. First, the flux $Q(S)$ is continuous at S^* , since the flow in the main basin only perceives the slower one at the lateral plains through the interface P_0 , and this has length zero when $S = S^*$. This contrasts sharply with the discontinuous flux predicted by the kinetic wave model with just one mean velocity. Second, the function $Q(S)$ is convex for $S < S^*$ and $S > S^*$, but has a slope discontinuity at S^* which makes it globally nonconvex (see Figure 12). The reason for this behavior is simple: as we cross the value S^* , the mean velocity U_1 keeps growing at about the same rate as before as a function of S_1 , but not as a function of $S = S_1 + S_2$. On the other hand, U_2 starts from zero, since for S only slightly

above S^* , the frictional forces are much larger than gravity in the flood plains. Then, $Q(S)$ will initially grow at a rate about b^+/b^- slower than before the flooding, since this is the quotient between the rates of growth of S and S_1 .

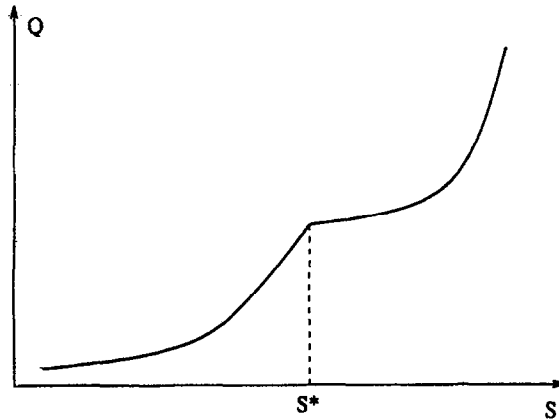


Figure 12. Flux function for a river with flood plains. The function is nonconvex, with a corner at the critical flood level S^* .

For a river trapped in a canyon, such as the one plotted in Figure 5, the assumption of existence of an approximately uniform mean flow is well founded, so the kinetic wave model applies without further refinements. The piecewise trapezoidal approximation is particularly well suited for this case, since there is a clear discontinuity in the lateral slopes when the bed of the river reaches the walls of the canyon. Therefore, we should expect a convex flux function with a sharp corner, such as the one plotted in Figure 13.

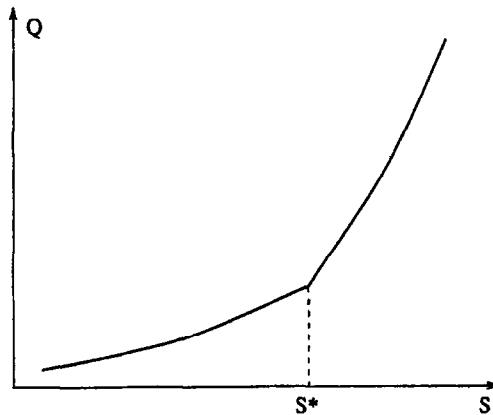


Figure 13. Flux function for a river trapped in a canyon. Convex function, with a corner at the critical level S^* , where the lateral walls meet the canyon.

We have found the qualitative features of the shape of the flux function for rivers with flood plains and rivers trapped in canyons. These are not only important examples themselves, but also work as prototypes for rivers and channels with sharp changes in the lateral slopes. The former illustrates the situation in which the slope decreases sharply with altitude, giving rise to a nonconvex flux, and the latter exemplifies those cases with sharply increasing slopes, which yield convex laws with corners. Qualitatively similar behaviors should be expected when sharp changes occur not in the lateral slopes, but in the roughness of the material of the bed. An increasing roughness has a similar effect to a decreasing slope, since both contribute to a larger lateral friction. In the following sections, we will see what consequences these shapes of the flux function have on the dynamics of floods.

5. THE RIEMANN PROBLEM FOR NONCONVEX FLUX FUNCTIONS

In this and the following section, we study the Riemann problem for scalar conservation laws with flux functions of the types arising in rivers with flood beds and rivers trapped in canyons. There are many reasons for considering the Riemann problem. On the one hand, any initial value problem with different values at plus and minus infinity looks like a Riemann problem when looked at from afar. Thus, for studying the qualitative features of a flood wave, it suffices to consider a Riemann problem with a larger value of S upstream, while the end of a flood is well described by a Riemann problem with S larger downstream. On the other hand, the Riemann problem is the main building block of most numerical algorithms for studying systems of conservation laws. In particular, we will describe in Section 7, a version of Godunov's second-order method particularly well suited to the study of laws with nonconvex or nonsmooth fluxes. Finally, the solution to a Riemann problem is very easy to describe, and sheds light on the most important qualitative consequences of the shape of the flux function.

The Riemann problem for equation (6) is the following: find the solution to (6) with initial conditions

$$S(x, 0) = \begin{cases} S_-, & \text{for } x < 0, \\ S_+, & \text{for } x > 0. \end{cases} \quad (12)$$

In our hydraulic context, S_- larger than S_+ corresponds to flooding, and S_- smaller than S_+ to a flood's end.

The solution to this Riemann problem is a function $S(\xi)$ of $\xi = x/t$ such that, whenever $S(\xi)$ is smooth,

$$\frac{dQ}{dS}(S(\xi)) = \xi,$$

and at points where the solution is discontinuous, the jump condition

$$\frac{Q(S(\xi^+) - Q(S(\xi^-)))}{S(\xi^+) - S(\xi^-)} = \xi$$

holds. These requirements do not determine the solution uniquely; some further constraints characterizing which shocks are admissible are also required (see [11]). However, if we specify that the solution to the Riemann problem be monotonic and stable under small perturbations to the initial data, a very simple recipe provides the solution to any scalar equation, with either convex or nonconvex flux function. This recipe works as follows (see Figure 14): if S_- is smaller [larger] than S_+ , draw the convex [concave] hull of $Q(S)$ between S_- and S_+ . Each point S where $Q(S)$ and its hull coincide corresponds to a point in the solution; its location is given by $x/t = \xi$, where ξ is the (possibly multivalued) slope of the hull at the point S . This slope coincides with $Q'(S)$ within a smooth rarefaction, while within shocks it yields the same shock velocity as the Rankine-Hugoniot jump condition.

Before providing a justification for this procedure, let us watch it in action in a simple situation. Consider the case of a convex flux function, where the solution to the Riemann problem is well known: if the characteristic velocity upstream is larger than the one downstream, the solution consists of a single shock between both states with $\xi = (Q(S^-) - Q(S^+))/(S^- - S^+)$; otherwise, a smooth rarefaction arises with $\xi = \frac{dQ}{dS}(S(\xi))$. But this is also the solution provided by the construction above, where the shock corresponds to the concave hull of $Q(S)$, and the rarefaction to its convex hull, which coincides with the function $Q(S)$ itself. Why could we not allow shock solutions in both cases? The answer is stability. Imagine we propose that the solution to all Riemann problems be a single shock separating the states up and downstream, with velocity given by $\xi = (Q(S^-) - Q(S^+))/(S^- - S^+)$. Consider the situation in which S^- is smaller than S^+ . We may divide the initial discontinuity between S^- and S^+ into two discontinuities, say (S^-, S) and (S, S^+) , and locate these slightly apart in the initial conditions. If we compute the velocities

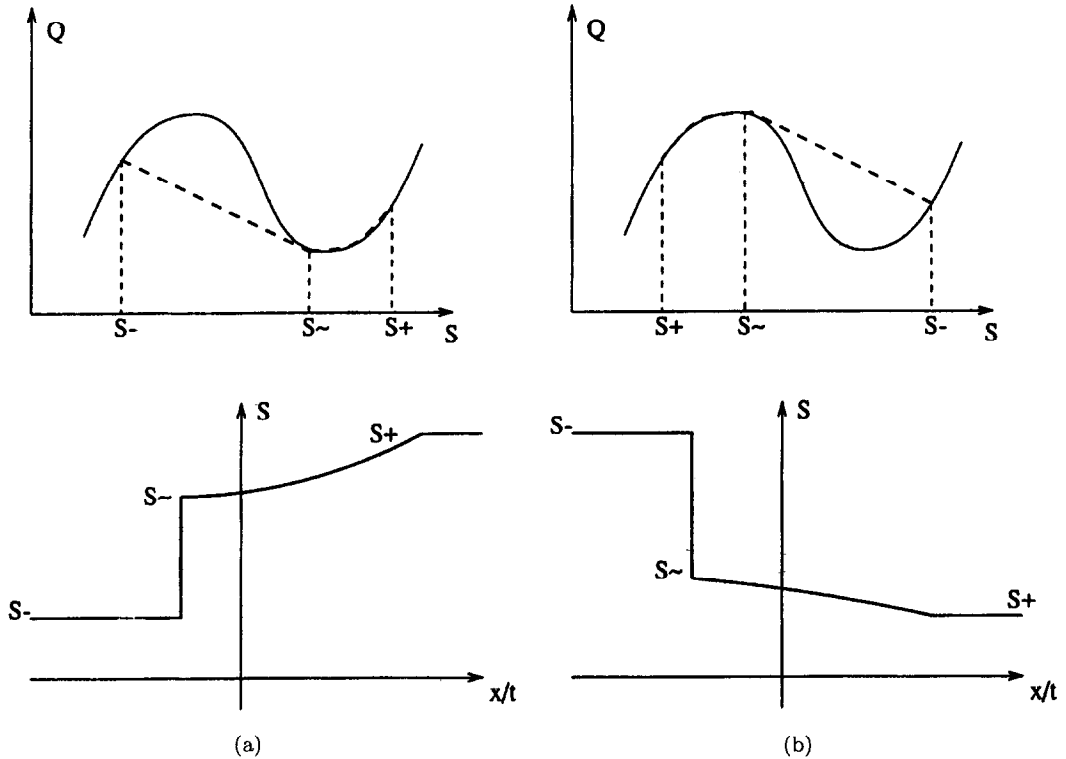


Figure 14. Riemann problem for a scalar conservation law with nonconvex flux function. Graphic construction of the solution, using convex or concave hulls of $Q(S)$.

of these two weaker shocks, we find that the one ahead moves faster than the one behind, so the distance between both increases linearly with time. But this means that the solution with a single shock was unstable under small perturbations to the initial condition, which makes it invalid.

Let us justify now the recipe given above. To this end, notice that it corresponds exactly to what one would require of the solution to the Riemann problem. One would seek a function $S(\xi)$ with the following features.

- (a) $S(\xi)$ is a monotonic function of ξ , defined between two values ξ_- and ξ_+ , with $S(\xi_-^-) = S_-$ and $S(\xi_+^+) = S_+$, where the superscripts denote limiting values from the left and right.
- (b) For each pair (ξ_1, ξ_2) with $\xi_- \leq \xi_1 \leq \xi_2 \leq \xi_+$, the following inequalities hold for all values of S between $S(\xi_1^-)$ and $S(\xi_2^+)$ and strictly different from both:

$$\frac{Q(S(\xi_2^+)) - Q(S)}{S(\xi_2^+) - S} \leq \xi_1 \leq \frac{Q(S(\xi_2^+)) - Q(S(\xi_1^-))}{S(\xi_2^+) - S(\xi_1^-)} \leq \xi_2 \leq \frac{Q(S) - Q(S(\xi_1^-))}{S - S(\xi_1^-)}.$$

Notice that, if we let ξ_1 and ξ_2 approach a common value ξ , the two inner inequalities become just one equality, which yields the jump condition for (6) if $S(\xi^-) \neq S(\xi^+)$ and the characteristic velocity $\xi = Q'(S(\xi))$ if $S(\xi)$ is smooth. The two outer inequalities act as stability conditions, which guarantee that, if we divide the interval $(S(\xi_1^-), S(\xi_2^+))$ into two subintervals with $(S(\xi_1^-), S)$ and $(S, S(\xi_2^+))$ and change the initial conditions so that those two subintervals start at points slightly apart, their separation will not increase as time progresses. In other words, the solution is at least neutrally stable. The simplest way to see this is to consider a shock between the states $S(\xi^-)$ and $S(\xi^+)$. If we pose as initial data two shocks $(S(\xi^-), S)$ and $(S, S(\xi^+))$ separated by a small distance, we would like these two shocks to eventually collide into a single one, or at least not to spread further apart. In addition, the shock ahead cannot move faster than the original compound shock, nor can the shock behind move more slowly, since either

case would violate conservation of S . But these are precisely the conditions in the inequalities above when $\xi_1 = \xi_2$. The general case with $\xi_1 \neq \xi_2$ follows from the particular case in which they coincide plus monotonicity.

Thus, conditions (a) and (b) are necessary. As they are equivalent to the previous characterization in terms of convex or concave hulls, and these hulls are unique, sufficiency follows immediately. Therefore, we have a very simple procedure to solve the Riemann problem, drawing the concave or convex hull of $Q(S)$ between S^- and S^+ , depending on whether S^- is larger or smaller than S^+ .

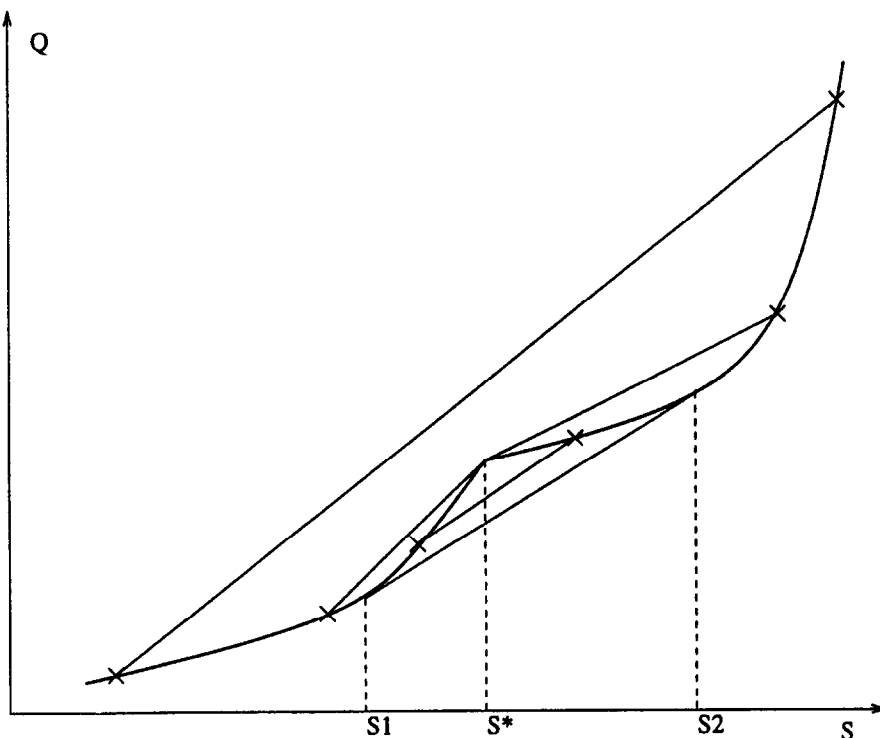


Figure 15. Convex and concave hulls of sections of the flux function for a river with flood plains.

6. QUALITATIVE FEATURES OF FLOODS AND FLOOD ENDS FOR RIVERS WITH FLOOD BEDS AND RIVERS TRAPPED IN CANYONS

We have shown in Section 5 a simple recipe for solving the Riemann problem for general scalar conservation laws. Now we will apply this recipe to the flux functions derived in Section 4, i.e., those of rivers with flood beds and rivers trapped in canyons.

The concave and convex hulls for the flux function corresponding to a river with flood plains are represented in Figure 15 for various values of S_- and S_+ , and the corresponding wave profiles are depicted in Figure 16. We see that strong flood waves propagate as one single shock, while weaker floods decompose into two shocks, of which the first makes the water level just reach the critical height beyond which flooding occurs, while the second raises the water all the way up to its highest level. The flood ends, on the other hand, propagate along a single discontinuity, isolated for weak floods and surrounded by smooth waves for stronger ones. In the latter case, the discontinuity connects two “conjugated heights,” with corresponding areas S_1 and S_2 , which are independent of the actual values of S_- and S_+ , and can be computed from the flux function alone. There are other cases, of course, which the reader can easily work out, with a smooth rarefaction occurring at only one end of the discontinuity.

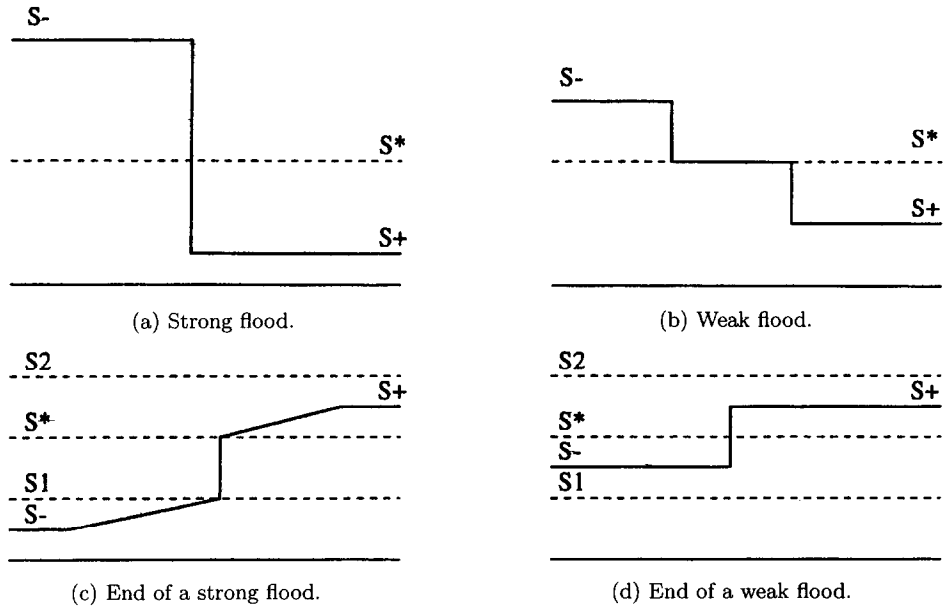


Figure 16. Solution to Riemann problems for a river with flood plains.

These results contrast sharply with those for rivers without irregularities, where floods are carried by single shocks and their ends by smooth rarefactions. Two predictions are particularly striking: that floods should arrive in two separate waves, the first of them barely filling up the river's main basin, and that floods should end suddenly, with a discontinuous drop in the level of water. Sharp discontinuities, of course, never occur in reality; a discontinuity in our simplified model should correspond to changes taking place on short scales relative to the river, which includes "shocks" a few kilometers wide! We do not know whether these phenomena have been observed in real floods, and would appreciate any relevant information. The only partial confirmation we have is that, in recent floods of the Magdalena River in Colombia, the inhabitants of the plains surrounding the river saw the floods come in two separate waves.

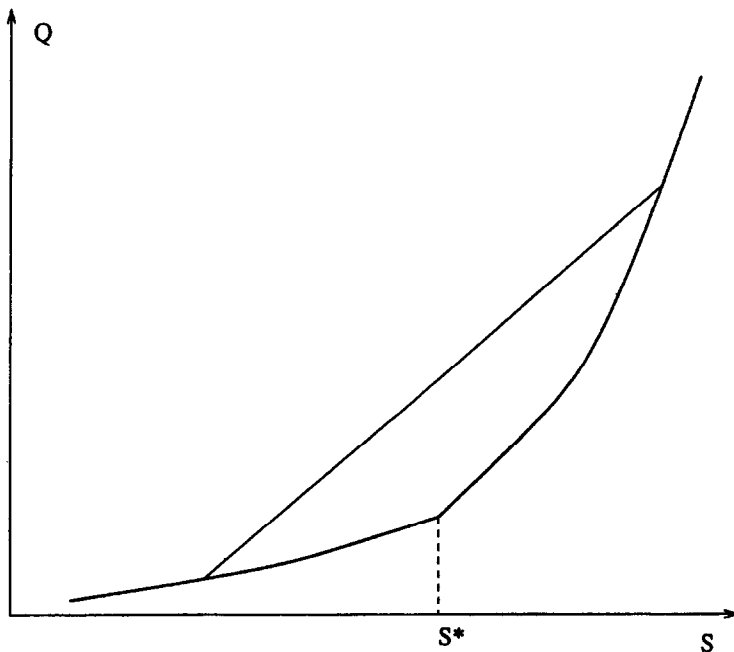


Figure 17. Convex hull of a section of the flux function for a river trapped in a canyon.

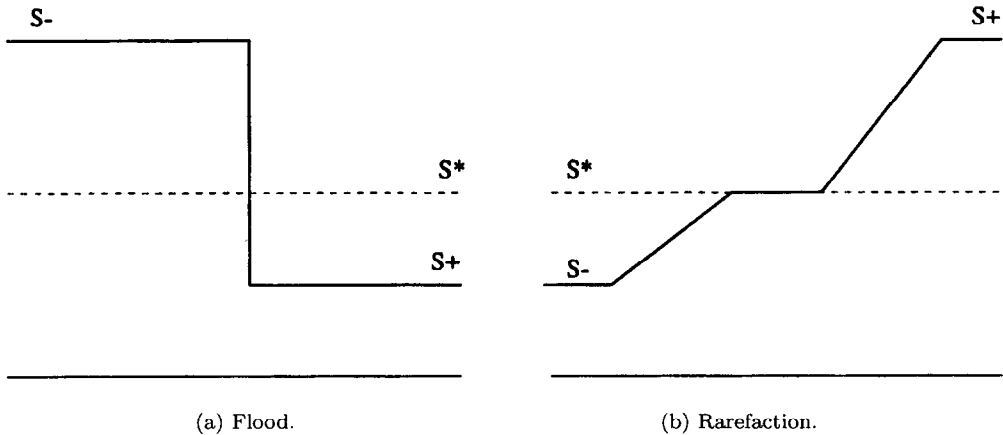


Figure 18. Solution to Riemann problems for a river trapped in a canyon.

Figure 17 shows the concave and convex hulls of the flux function associated with rivers trapped in canyons, and Figure 18 depicts the corresponding waves. In this case, floods take place always along single shocks, while the flood ends decompose into two rarefactions, separated by a region where the water level is exactly at the height where the bed of the river reaches the walls of the canyon. This latter phenomenon, though surprising, is far less striking than those predicted above for rivers with flood plains. Yet it would be interesting to know how accurately it corresponds to reality.

7. A SECOND-ORDER GODUNOV METHOD FOR SCALAR CONSERVATION LAWS WITH NONCONVEX OR NONSMOOTH FLUX FUNCTIONS

The characterization of the solution to a Riemann problem in terms of convex or concave hulls proposed in Section 5 has an interesting numerical corollary: we may build Riemann solvers for scalar equations based solely on drawing hulls of discretized versions of the flux function $Q(S)$. We will see in this section how this fact allows us to design an algorithm for solving scalar conservation laws particularly well suited for flux functions which are either nonsmooth or nonconvex, and either have a complicated analytical structure or are known only at a discrete set of points. Such an algorithm is ideal for flood routing models, since the discharge/surface level relations for rivers are empirical functions given in form of tables, and any irregularity in the cross-section of the river translates into nonsmoothness and often nonconvexity of the flux function.

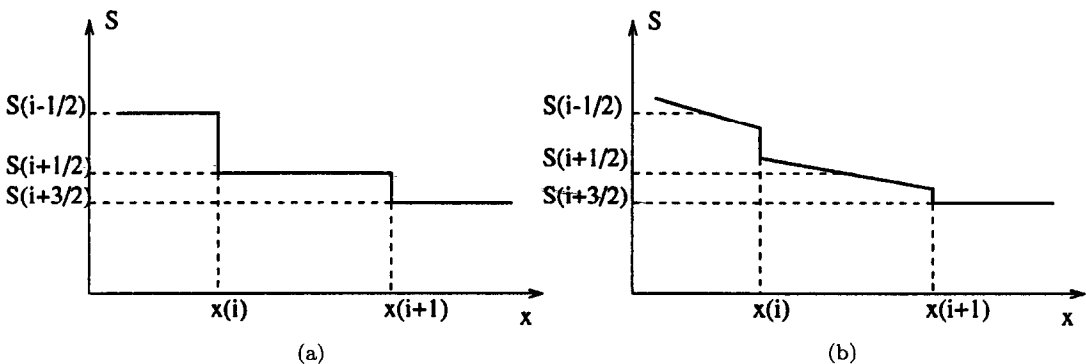


Figure 19. Interpolations for first-order and second-order Godunov.

For completeness, let us describe briefly the first-order and second-order Godunov methods for scalar conservation laws, and then show the way we propose to implement the Riemann solver,

which is a crucial building block for both. Godunov's original method [12] is based on a very simple, yet extremely rich and robust idea. In the context of equation (6), the method reduces to the following procedure. Given the initial data $S(x, 0)$ and a grid x_i , replace S by a piecewise constant function, with a value on each interval (x_i, x_{i+1}) equal to the average $S_{i+1/2}$ of $S(x, 0)$ over the interval (Figure 19a). In order to update these average values at time Δt , we need to integrate over time the flux $Q(S)$ at each point x_i . Then

$$S_{i+1/2}(\Delta t) = S_{i+1/2}(0) + \frac{1}{x_{i+1} - x_i} \int_0^{\Delta t} (Q(x_i, t) - Q(x_{i+1}, t)) dt.$$

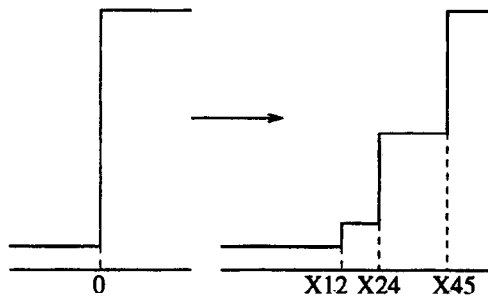
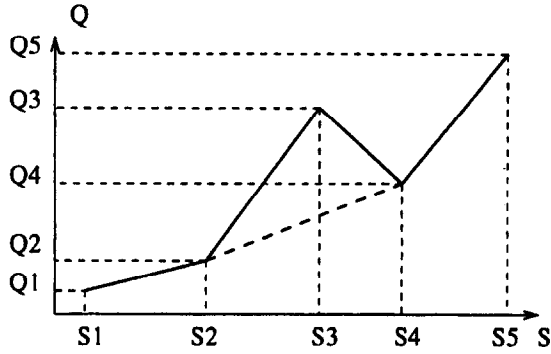
But, for Δt small enough that information from noncontiguous cells does not interact, Q is constant at each point x_i , with a value equal to $Q(S_*)$, where S_* is the solution at $\xi = 0$ of the Riemann problem between states $S_{i-1/2}$ and $S_{i+1/2}$.

In the second-order version of the algorithm (see [13]), the data with which we start each step are still the averages $S_{i+1/2}$ over the grid. However, these averages are used to build a piecewise linear, instead of piecewise constant, initial state (Figure 19b). The slopes at each cell are normally computed using central differences, with additional monotonicity constraints designed to avoid spurious oscillations. Equivalent reconstructions of piecewise linear functions can be obtained from ENO schemes [14]. Now Q is no longer constant at each grid-point; its integral over time arises from the solution to a generalized linear problem between two linear states, which can be computed solving standard Riemann problems (see [15]). The reduction to a standard Riemann problem is particularly simple for scalar conservation laws.

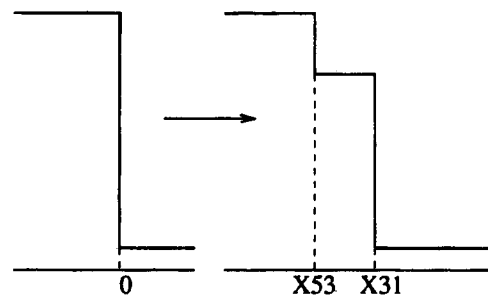
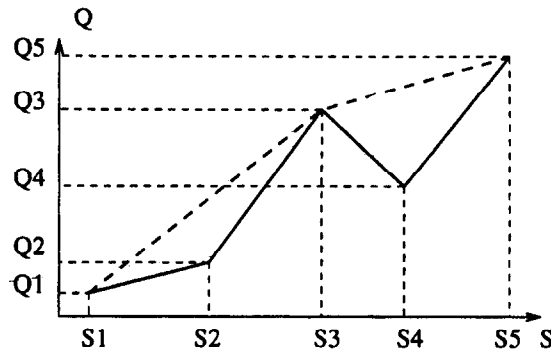
The generalization of these procedures to moving grids with local space and time refinements is relatively straightforward [15]; moving grids are useful for flood routing, since flood waves of the type studied in this paper move downstream.

Let us describe the proposed Riemann solver for scalar conservation laws with irregular flux functions. According to the results of Section 4, in order to solve the Riemann problem between S_- and S_+ , it suffices to draw the convex or concave hulls of $Q(S)$ between S_- and S_+ , depending on whether S_- is larger or smaller than S_+ . The idea of the numerical solver proposed here is to replace the flux function $Q(S)$ between S_- and S_+ by a piecewise linear function, for which the computation of hulls is almost trivial. We will discuss below the best way to perform this discretization of the flux function. In Figures 20a and 20b, we assume that the discretization is given, and illustrate the construction of the convex and concave hulls and the solution of the corresponding Riemann problems. The interval between S_- and S_+ has been divided into four subintervals $(S_1, S_2), \dots, (S_4, S_5)$, with $S_1 = S_-$ and $S_5 = S_+$ if $S_- < S_+$ (Figure 20a) and $S_1 = S_+$ and $S_5 = S_-$ otherwise (Figure 20b). The flux $Q(S)$ has been replaced by a continuous piecewise linear function, with the correct value of Q at each of the S_i 's. Finding the convex or concave hull of these piecewise linear functions becomes a very simple combinatorial problem. For the convex [concave] hull, we start at S_1 , look at all the S_i 's ahead, and choose the S_{i^*} that minimizes [maximizes] the speed $\xi_{1i} = (Q(S_i) - Q(S_1))/(S_i - S_1)$. In the solution to the Riemann problem, S will have the value S_1 to the left [right] of this value of ξ , where it will jump to S_{i^*} . Then we replace S_1 by S_{i^*} , and repeat the procedure until we reach S_5 .

Therefore, for a given a discretization of $Q(S)$, the process of solving the Riemann problem is extremely simple. The next question is what discretization should be chosen. The precision of the solution, of course, increases with the number of points in the discretization. Nevertheless, *the Riemann solver preserves the order of accuracy of the Godunov method of which it makes part, even if no points are taken between S_- and S_+ , i.e. if $Q(S)$ is locally replaced by a linear function.* The reason for this fact is that, in locations where the solution is smooth, the difference between S_- and S_+ is $O(\Delta x)$ for a first-order Godunov and $O(\Delta x^2)$ for a second-order Godunov, so the errors committed in approximating $Q(S)$ by a linear function fall within the accuracy of the method. Notice that using a locally linear $Q(S)$ corresponds to giving always a shock as



(a)



(b)

Figure 20. Construction of convex and concave hulls of a discrete version of a non-convex flux function, and corresponding discrete solution to Riemann problems.

the solution to the Riemann problem. Unphysical “rarefaction shocks” do not survive though, since the averaging intrinsic to Godunov automatically creates intermediate values inside these unstable discontinuities, making them spread out. Only a “rarefaction shock” sitting on a grid point will avoid averaging, but such event has probability zero.

Yet we do not advocate such an extreme solution. Our claim is that, with little more computational effort, huge gains can be obtained. The reasons are twofold: we would like strong waves to

be accurately represented, and we would like distinguished values of S , as S^* in rivers with flood plains, to be singled out immediately in the numerical solution, as they are in the exact solution to the equations. Take this latter example first. We know, from the results of Section 6, that not too strong flood waves decompose into two shocks, separated by a growing interval where S equals S^* . If we let Godunov's averaging do the job of picking up intermediate values between S_- and S_+ , the solution will certainly converge to the right one with two shocks, but in a far less sharp way than would be desirable. The values between the two shocks, for instance, will get closer and closer to S^* , but never quite hit it exactly. On the other hand, if we single out S^* by the harmless trick of including it as an intermediate value between S_- and S_+ in the Riemann solver described above, the solution between the two shocks will reach $S = S^*$ in finite time. Similarly, a strong wave will be far more accurately resolved if a few points are inserted between S_- and S_+ for the corresponding Riemann problems. This is particularly true for flux functions with corners or inflection points, where the Riemann problem has a solution much richer than a simple shock or rarefaction.

Therefore, the two following general principles should guide the choice of the local discretization of $Q(S)$: make sure not to skip any distinguished value of S , as those corresponding to corners or inflection points of $Q(S)$, and always insert a few points within a Riemann problem with a large initial discontinuity. Further details are problem and taste dependent. If $Q(S)$ is provided in the form of a table, for instance, no further discretization is required. If $Q(S)$ is expensive to compute, we may want to have a global discretization, computed only once, independent of the actual values of S_- and S_+ ; for each Riemann problem, then, only $Q(S_-)$ and $Q(S_+)$ need to be computed. On the other hand, if $Q(S)$ is cheap to compute, we may adopt an almost uniformly distributed grid for each pair (S_-, S_+) , only slightly distorted to accommodate distinguished points. This is the policy we adopted for the numerical experiments in the following section. The discretization procedure is sketched in Figure 21. The input parameters are S_- , S_+ , the approximate number n of subintervals desired (five in the figure) and a table of distinguished values of S . If none of these values falls within (S_-, S_+) , the interval is simply divided uniformly into n subintervals (Figure 21a). If one or more distinguished values fall within the interval (they are marked with crosses in Figures 21b and 21c), the discretization is distorted slightly so as to make them fit. Sometimes (Figure 21c), the distortion becomes big enough that the tolerance for the width of the subintervals is reached, and one or more extra points are added.

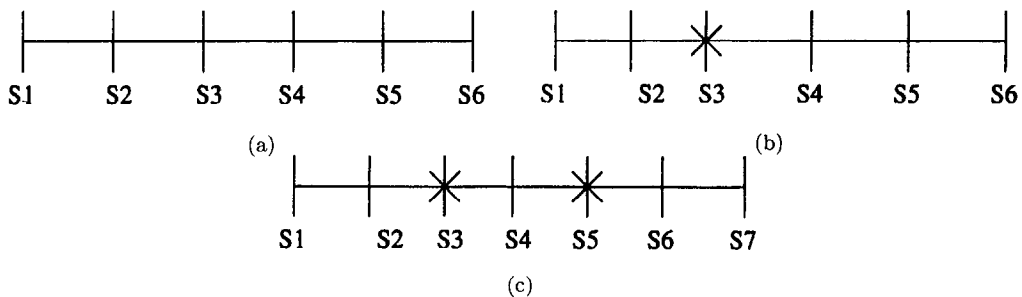


Figure 21. Choice of intermediate points in a discretization of the flux function between two values of S . The crosses mark distinguished points, which the discretization must include.

8. TWO NUMERICAL EXAMPLES

The description in Section 6 of the qualitative behavior of floods and their ends for rivers with flood plains and rivers trapped in canyons was based on the solution to the Riemann problem. Yet it can be argued that Riemann problems seldom occur in real floods, except perhaps when dams break. In this section, we justify our assertion that Riemann problems do nonetheless capture the qualitative behavior of floods and flood ends, by carrying out numerical simulations

of the kinematic model (6) for more general initial data. These numerical experiments serve the additional purpose of illustrating the algorithm described in Section 7.

We adopted as an idealized flux function $Q(S)$ for a river with flood plains, the piecewise Burgers-like definition

$$Q(S) = \begin{cases} S^2, & \text{for } S < 1, \\ \frac{S^2 + 1}{2}, & \text{for } S > 1, \end{cases} \quad (13)$$

which agrees qualitatively with the one plotted in Figure 12, with the critical level S^* beyond which flooding occurs normalized to one. Similarly, for a river trapped in a canyon, we took the function

$$Q(S) = \begin{cases} \frac{S^2}{2}, & \text{for } S < 1, \\ S^2 - 0.5, & \text{for } S > 1, \end{cases} \quad (14)$$

similar to the one plotted in Figure 13. In both cases, for simplicity, we adopted a periodic domain between zero and one, and the smooth initial condition

$$S(x, 0) = 0.8 + 0.5 \sin(2\pi x), \quad (15)$$

which has a segment over flooding level. Equation (6) was solved using the algorithm of Section 7, with 200 grid points, and time intervals $\delta t = 0.001$. For each Riemann problem, four points were used to interpolate the flux function $Q(S)$. The results of these two runs are displayed in Figures 22 and 23.

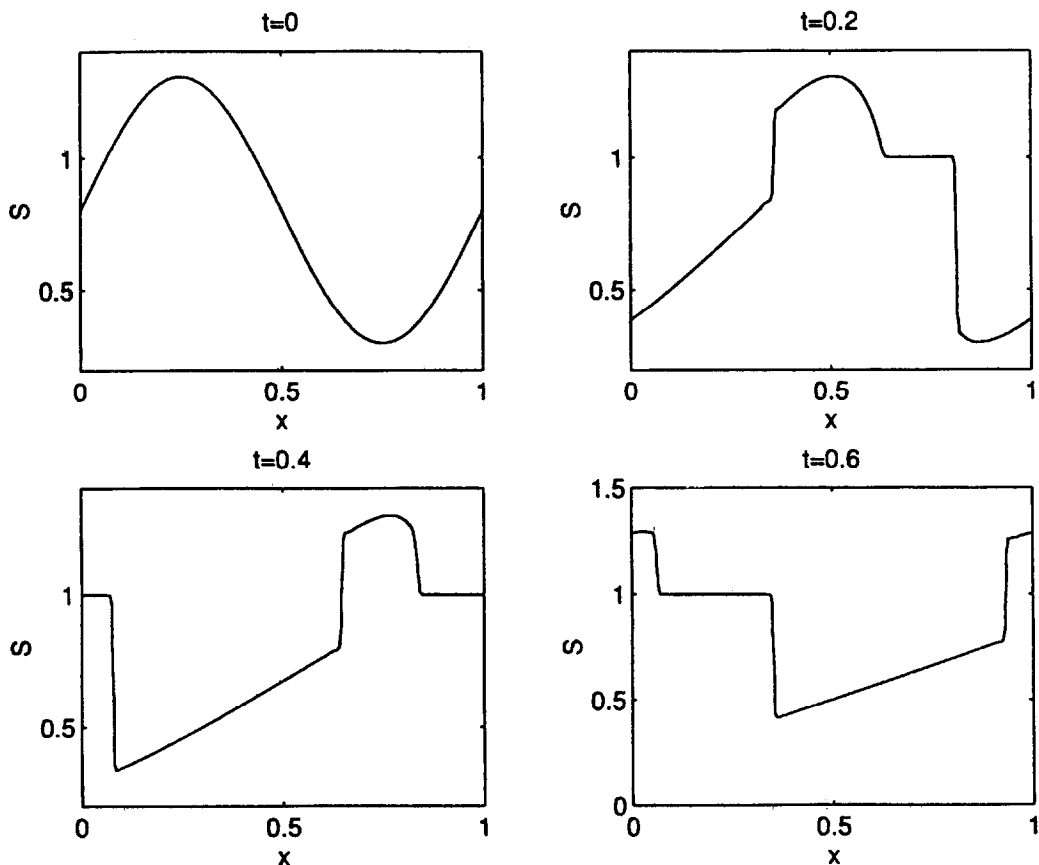


Figure 22. Numerical solution to the kinematic model for a river with flood plains, on a periodic grid.

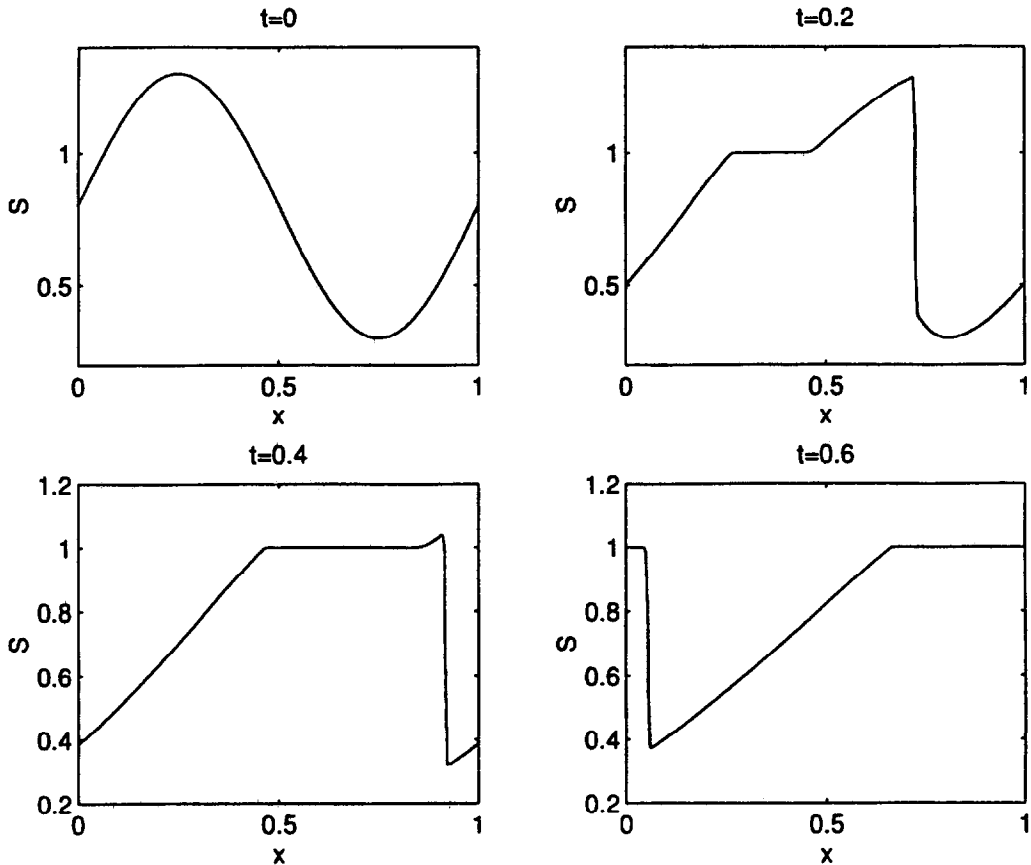


Figure 23. Numerical solution to the kinematic model for a river trapped in a canyon, on a periodic grid.

Figure 22 contains four snapshots of the solution to (6) with flux function (13), corresponding to a river with flood plains. At time $t = 0$, we have the initial condition (15). At time $t = 0.2$, the flood wave has already decomposed itself into two waves, separated by a region with constant cross-section S^* . One of these waves has already broken into a hydraulic jump; the other is about to break. The wave announcing the end of the flood, on the other hand, has from time $t = 0^+$ developed a jump which, by the time $t = 0.2$, has grown to an appreciable strength. At time $t = 0.4$, all waves are fully developed, the two flood jumps, the constant solution in between, and the jump at the end of the flood. Finally, at time $t = 0.6$, we start to see decay due to the dissipation at the hydraulic jumps. Notice that even the “rarefaction jump” dissipates energy, since it has the mathematical structure of a shock.

The same snapshots for the flux function (14), corresponding to a river trapped in a canyon, are displayed in Figure 23. The initial condition of time $t = 0$ has, by the time $t = 0.2$, already developed a strong flood jump, with the rarefaction behind it decomposed into two waves, separated by a constant state $S = S^*$. At time $t = 0.4$, the segment with $S > S^*$ has been dissipated away almost completely at the jump, while the constant part of the solution has kept growing in size. By the time $t = 0.6$, the flooded region has totally vanished, which leaves us with a standard inviscid Burgers’ equation for the rest of the flow, with an unusual flat region in the initial data.

9. CONCLUSIONS

The simplest possible kinematic model for rivers with irregular geometries yields surprising predictions. For rivers with flood plains, these predictions are particularly striking; they imply that flood waves should decompose into two hydraulic jumps, separated by a growing region

where the water-level is constant and has the critical flooding value. The end of a flood, on the other hand, should take the form not of a rarefaction wave, but of an inverted hydraulic jump. If verified experimentally, these predictions could have practical consequences in our ability to deal with catastrophic floods.

The mathematics behind these predictions is that of scalar conservation laws with nonconvex flux functions. The structure of the Riemann problem for such equations was discussed, and a conservative numerical method was proposed to deal with more general initial data.

A natural continuation of the work described in this article would be the study of rivers with irregular geometries in the more complete setting of the Saint-Venant equations (1),(2). We anticipate that the corrections to the simplified model just presented will be most significant in the vicinity of hydraulic jumps. However, the main features of the solutions described here should remain basically unchanged.

REFERENCES

1. J.J. Stoker, *Water Waves*, Wiley, New York, (1957).
2. J.-A. Liggett and J.-A. Cunge, Numerical methods of solutions of unsteady flow equations, In *Unsteady Flow in Open Channels*, Vol. I (Edited by K. Mahmood and V. Yevjevich), pp. 89–178, Water Resources Publications, Fort Collins, CO, (1975).
3. M.J. Lighthill and G.B. Whitham, On kinematic waves I (Flood movements in long rivers), *Proc. Roy. Soc. A* **229**, 281–316 (1955).
4. D.K. Borah, M.S. Ashraf and V.S. Neary, Kinematic wave based hydrologic models with different solution methods, In *Hydraulic Engineering* (Edited by H.H. Chang and J.C. Hill), pp. 421–426, ASCE, (1990).
5. A.A. Bradley and K.W. Potter, Estimating floodplain limits for complicated hydrologic and hydraulic conditions, In *Engineering Hydrology* (Edited by C.Y. Kuo), pp. 575–580, ASCE, (1993).
6. M.H. Gradowczyk, P.M. Jacovkis, A. Tamusch and F.M. Diaz, A hydrological forecasting model of the Uruguay River basin system, In *Hydrological Forecasting (Proceedings of the Oxford Symposium)*, pp. 517–524, IAHS Publ., (1980).
7. U.S. Army Corps of Engineers, *HEC-1, Flood Hydrograph Package: Users Manual*, Hydrological Engineering Center, Davis, CA, (1985).
8. A.F. Pabst, Next generation HEC catchment modeling, In *Engineering Hydrology* (Edited by C.Y. Kuo), pp. 1013–1018, ASCE, New York, (1993).
9. P.M. Jacovkis, Modelos hidrodinámicos en cuencas fluviales, *Revista Internacional de Métodos Numéricos para Cálculo y Diseño en Ingeniería* **5**, 295–320 (1989).
10. P. Lax, *Hyperbolic Systems of Conservation Laws and the Mathematical Theory of Shock Waves*, Society for Industrial and Applied Mathematics, Philadelphia, PA, (1973).
11. D.P. Ballou, Solutions to nonlinear hyperbolic Cauchy problems without convexity conditions, *Trans. Am. Math. Soc.* **152**, 441–460 (1970).
12. S.K. Godunov, A finite difference method for the numerical computation of discontinuous solutions of the equations of fluid dynamics (in Russian), *Mat. Sb.* **47**, 357–393 (1959).
13. B. van Leer, Towards the ultimate conservative difference scheme II. Monotonicity and conservation combined in a second order scheme, *J. Comp. Phys.* **23**, 263–275 (1974).
14. A. Harten, S. Osher, B. Engquist and S. Chakravarthy, Some results on uniformly high-order accurate essentially nonoscillatory schemes, *Appl. Numer. Math.* **2**, 347–377 (1986).
15. E.G. Tabak, A second order Godunov method on arbitrary grids, *J. Comp. Phys.* (1996) (to appear).
16. J. Smoller, *Shock Waves and Reaction-Diffusion Equations*, Springer, New York, (1983).